Proceedings of the ASME 2012 10th International Conference on Nanochannels, Microchannels and Minichannels
ICNMM2012
July 8-12, 2012, Rio Grande, Puerto Rico

ICNMM2012-73224

EVAPORATION-INDUCED CASSIE DROPLETS ON SUPERHYDROPHILIC MICROSTRUCTURED SURFACES

Solomon Adera[1], Rishi Raj[1], Ryan Enright[1,2], and Evelyn N. Wang[1]

[1]Department of Mechanical Engineering
Massachusetts Institute of Technology
Cambridge, MA, 02139 USA

[2]Stokes Institute
University of Limerick
Limerick, Ireland

ABSTRACT

A droplet deposited on a rough, lyophilic surface satisfying the imbibition condition, results in complete wetting. However, in this work, we demonstrate that this behavior can be altered by superheating the substrate such that droplets can reside in a non-wetting Cassie state due to evaporation. Photolithography and deep reactive ion etching were used to fabricate a well-defined silicon micropillar array with diameter, height, and center-to-center spacings of 5.3, 21.7 and 27.5 μm, respectively. Water droplets placed on this microstructured surface at room temperature demonstrated superhydrophilic behavior with liquid filling the voids between pillars resulting in a vanishing contact angle. However, when the microstructured surface was superheated above a critical value, the superhydrophilicity was lost and non-wetting Cassie droplets were formed. The superheat required to deposit a Cassie droplet (>75˚C) was found to be significantly higher than that required to sustain an already deposited Cassie droplet (<35˚C). Interestingly, the superheat required to sustain a Cassie droplet after the initial deposition was found to decrease with the square of the droplet radius. These observations where an inherently superhydrophilic structured surface turns into superhydrophobic at nominal superheats has implications for phase change based heat transfer applications where the loss of contact between the substrate and the heat transfer fluid can be detrimental to the device performance.

NOMENCLATURE

Symbols

a	capillary length ($a = \sqrt{\rho_{liq} g/\sigma}$) (-)
Bo	Bond number ($Bo = g(\rho_{liq} - \rho_{vap})R_0^2/\sigma$) (-)
d	pillar diameter (m)
F	force (N)
g	acceleration due to gravity (m/s^2)
H	sample thickness (m)
h	pillar height (m)
h_{fg}	latent heat of vaporization (J/kg)
K	permeability (m^2)
k	thermal conductivity (W/m-K)
l	pillar center-to-center spacing (m)
N	number of pillars (-)
P	pressure (N/m^2)
q''	heat flux (W/m^2)
r	radial coordinate
rf	roughness ratio ($rf = 1 + \pi dh/l^2$) (-)
R	droplet base radius (m)
R_0	droplet major radius (m)
T	temperature (˚C)
ΔT	superheat, (T_s - T_{sat}) (˚C)
u	vapor radial velocity (m/s)
v	vapor z-direction velocity (m/s)
V	droplet volume (L)
z	surface normal coordinate

Greek

ε	porosity ($\varepsilon = 1 - \pi d^2/4l^2$) (-)
μ	dynamic viscosity (Ns/m^2)
θ	contact angle (˚)
ρ	density (kg/m^3)
σ	surface tension (N/m)
ϕ_s	solid fraction ($\phi_s = \pi d^2/4l^2$) (-)

Subscripts

amb	ambient
app	apparent

c	apparent
down	downward
eff	effective
f	flat
imb	imbibition
liq	liquid
p	pillar
s	surface
sat	saturation
si	silicon
up	upward
vap	vapor

INTRODUCTION

Fundamental understanding of solid-liquid interactions is important for wettability control and the design of surfaces with functional properties. For some applications, it is desired that a droplet deposited on a solid surface spreads spontaneously making a thin film. Anti-fogging surfaces utilize this behavior to mitigate the formation of light-scattering droplets in order to maintain transparency [1]. Heat pipes, where wicking of condensate is required for better thermal management, is another example that utilizes the affinity of liquids to wet a surface. On the other end of the spectrum, dropwise condensation requires the drops to be non-wetting to minimize thermal resistances. Non-wetting droplets are also desired in chemical and biological applications where contamination of the solid surface is undesirable. Other applications include low-friction hydrodynamic surfaces where apparent hydrodynamic slip improves performance [1].

Wettability of solid surfaces can be tuned by introducing roughness [1-3]. This effect has been demonstrated since the 1940's [4-5] whereby texturing increases the degree of hydrophilicity (hydrophobicity) of an inherently hydrophilic (hydrophobic) flat surface and can be understood in terms of energy minimization [1, 6]. Depending on the history and the deposition technique, a droplet typically demonstrates one of two states on a rough surface: Wenzel or Cassie [3, 7]. In the Wenzel state a droplet wets the entirety of the droplet basal area by filling the surface asperities whereas a droplet in the Cassie state sits on top of the rough structure with air trapped between the asperities [1,3,7]. The wetting state with the lowest free energy is generally favored. However, metastable states are also possible [7]. Cassie and Wenzel drops exhibit significantly different wetting characteristics and have been extensively studied in the past with special emphasis on understanding the transition between the two states [8-10].

The Cassie-to-Wenzel transition can be induced by applying external stimuli such as vibration, pressure, electric fields, or thermal excitation. Vibration-induced Cassie-to-Wenzel transition on rough surfaces was studied by Bormashenko *et al.* [11, 12]. They reported that the resulting force per unit length on the triple line is responsible for the Cassie-to-Wenzel wetting transition and that the apparent contact angle is dictated by the interactions occurring at the three-phase contact line. Han *et al.* [13] investigated Cassie-to-Wenzel transition for a superhydrophobic CNT-based nanocomposite surfaces by applying a potential difference between the water droplet and the solid surface (electrowetting). In another work, Krupenkin *et al.* [14] investigated both theoretically and experimentally the fully reversible wetting-dewetting transitions of droplets on electrically tunable superhydrophobic nanostructured surfaces. Liu *et al.* [15] reported the transition of water droplets from Wenzel-to-Cassie state on a hydrophobic microstructured surface either by heating the substrate or by directly heating the droplet using a pulsed laser. The water infiltration dynamics during evaporation triggered wetting transition of a droplet from non-wetting to wetting state on transparent hydrophobic microstructured surfaces was studied by Tsai *et al.* [16]. They demonstrated that a natural evaporation process can drive the wetting transition in hydrophobic miscrostructured surfaces if the droplets are below a few hundreds of micron in radius. Zhang *et al.* [17] experimentally studied the effect of temperature on the wetting transition of droplets from spreading (wetting) to bouncing (non-wetting) on micro- and nanostructured surfaces.

A smooth, flat silicon surface is inherently hydrophilic. Its wettability is further improved through structuring and can exhibit superhydrophilic behavior at room temperature *i.e.* droplets instantaneously spread on the rough surface with vanishing contact angle demonstrating complete wetting, provided that the imbibition condition is satisfied [1, 2]. However, in this work, we demonstrate that when the same silicon surface is heated above a critical superheat, it exhibits superhydrophobic behavior with apparent contact angles as high as 150˚. This observed behavior might be a disadvantage for heat transfer applications that rely on actual contact between the heated surface and the working fluid. Such applications that utilize the latent heat of vaporization of the fluid include spray cooling of hot metals during metallurgical processes, cooling of nuclear reactors during emergency shutdown, heat exchangers, and cooling of overheated components in high-power-density thermal applications. Of central concern in these applications is whether an impinging droplet will wet the heated surface or will it bounce back without wetting. The effectiveness of these cooling applications relies on understanding the wetting behavior of droplets and their transition from one form to another. Understanding the Cassie-to-Wenzel transition with superheat would help formulate design guidelines for texturing surfaces with special wetting characteristics as desired for the specific phase-change based heat transfer applications.

EXPERIMENT

To explore the behavior of droplets deposited on hydrophilic microstructured surfaces, photolithography and deep reactive

ion etching were used to fabricate well-defined silicon pillar-arrays shown schematically in Fig. 1.

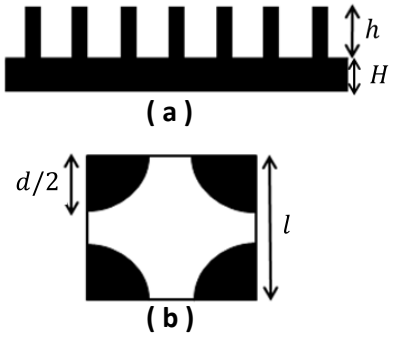

FIGURE 1: Schematic (not to scale) of (a) side and (b) top view of the microstructured surface used in the experiment showing the pillar diameter d, pillar height h, pillar center-to-center spacing l, and sample thickness H.

We studied a square array of pillars with d = 5.3 µm, h = 21. 7 µm, l = 27.5 µm, roughness ratio $rf = 1.48$, and solid fraction ϕ_s = 0.03. An SEM image of the microstructured surface at 30° inclination is shown in Fig. 2a. The geometry was chosen such that the imbibition condition as defined by Eq. 1 was satisfied [1, 2],

$$\cos\theta_{imb} = \frac{1-\phi_s}{rf-\phi_s}, \qquad (1)$$

where θ_{imb} is the critical angle below which the droplet spreads filling the void between pillars (wicking) following the surface asperities. For the microstructured surface under investigation, the imbibition angle θ_{imb} was calculated to be 48˚ while the intrinsic Young contact angle for smooth silicon surface was θ_{Si} = 38˚suggesting that a droplet should spread upon touching the structured surface.

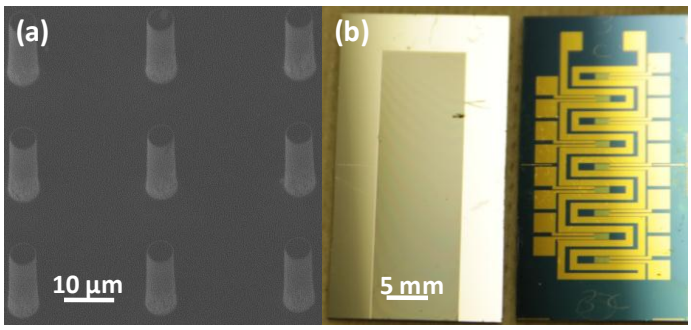

FIGURE 2: (a) SEM image of a microstructured surface (b) Image of front and back side of a typical surface used for the experiment, showing the microstructured surface and the back side gold resistive heater respectively.

A gold resistive heater (Fig. 2b) was patterned onto the backside of the silicon sample using ebeam evaporation. A DC power source was used to heat the sample and the temperature was measured at a rate of 10 Hz using a T-type thermocouple (TC) attached to the backside of the sample using thermal grease (3G Cool Silver, AI Technology) and Kapton tape.

Before each experiment, the samples were cleaned with acetone, methanol, isopropanol and deionized (DI) water; dried with nitrogen gas; and then oxygen plasma treated for 30 minutes to remove organic contaminants. After the plasma cleaning procedure, the surface was observed to be superhydrophilic and droplets spontaneously spread upon the surface with near zero contact angle. Thoroughly degassed DI water was used for all experiments to avoid gas bubble nucleation. A pipette was used to gently dispense droplets with volumes between 15 and 25 µL on the heated substrate. A 25 µm diameter gold wire, functionalized in a 1 mM ethanol solution of 1H, 1H, 2H, 2H-perfluorodecanethiol (Sigma-Aldrich), was used to keep the highly mobile droplets in position for visualization. The thiol coating made the intrinsically wetting gold wire hydrophobic, minimizing the component of surface tension acting in the vertical direction. Nonetheless, assuming the worst scenario (complete wetting of the gold wire), the force pulling the droplet up would be two orders of magnitude smaller than the other key forces involved in the evaporation-induced wetting transition phenomenon reported in this work.

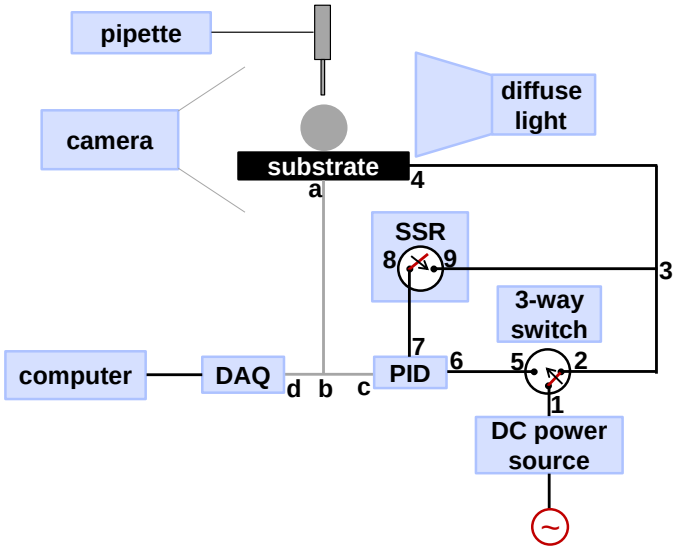

FIGURE 3: Schematic of the experimental setup (not to scale) that is used to study evaporation induced Cassie-to-Wenzel transition of water droplets. Junctions a-b-c-d represent thermocouples while 1-2-3-4-5-6-7-8-9 represent electrical wires and connections. The TC reading coming through a-b splits at junction b and c goes to the PID controller while d goes to the data acquisition.

As discussed previously, the superheat required to suspend a Cassie droplet on top of the structured surface was higher than that required to sustain the wetting state of an already

deposited droplet. This required a strategy (Fig. 3) that would allow the substrate to be maintained at two distinct steady state temperatures: a higher temperature initially and a relatively lower temperature after droplet deposition. As shown in Fig. 3, the substrate was initially heated directly (PID bypassed, 1-2-3-4, Fig. 3) such that a high superheat required for depositing a Cassie droplet was maintained. Once the droplet was deposited on the substrate, the superheat was lowered by toggling the 3-way switch from 2 to 5 such that the PID was brought into the loop (1-5-6-7-8-9-3-4, Fig. 3). The PID sensed the temperature through the thermocouple a-b-c and the SSR was shut-off allowing the substrate to cool down. Once the substrate cooled down and the temperature was lower than the set point on the PID (corresponding to the lower superheat required), a pulse was sent to SSR closing the circuit (through connection 8-9, Fig. 3) and the substrate was heated. The temperature from this point onwards was maintained at a steady value until the droplet transitioned to a Wenzel state or evaporated completely. In order to visualize the droplet behavior and understand the mechanism involved during transition, images were acquired at 10 fps during each of the experiments. The image and temperature data were later synchronized to closely investigate the wetting dynamics of droplets deposited on superheated substrates. The droplet volume, diameter and apparent contact angle were calculated by processing the captured images and temperature data through a custom analysis routine written in MATLAB®. A typical image of a droplet suspended on top of the micropillar array under superheated conditions is shown in Fig. 4. The apparent contact angle (θ_{app}) as measured from the inset image was 149˚ ± 2˚.

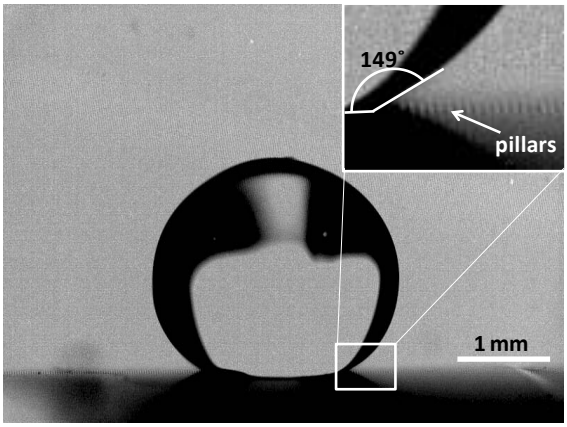

FIGURE 4: Image of an evaporating water droplet suspended on top of an array of pillars. The inset image shows the micropillar array and apparent contact angle, θ_{app} = 149˚ ± 2˚ measured from the acquired image.

RESULTS AND DISCUSSION

Owing to improved surface wettability due to microstructuring, droplets were observed to wet the surface completely (Fig. 5a) at low superheats. However, a non-wetting Cassie droplet on top of the microstructured surface was observed at a superheat of 90˚C (Fig. 5b). This critical superheat above which a non-wetting Cassie droplet formed was very sensitive to the droplet deposition technique and volume. As a result, ten experiments were performed at each superheat to investigate the repeatability of dispensing a non-wetting Cassie droplet and to obtain the range within which either of the two states existed. This result is shown on Fig. 6 where the percentage of Cassie droplets obtained out of ten experiments is shown at each superheat. All droplets deposited below 63˚C superheat wetted the surface (Wenzel state) while a non-wetting Cassie droplet was formed at all times if the superheat was higher than 75˚C. Between 63˚C and 75˚C superheat, a droplet could be in either state (Wenzel or Cassie) depending on how gently it was placed on the surface [7]. However, the probability of depositing a non-wetting Cassie droplet monotonically increased as the superheat increased.

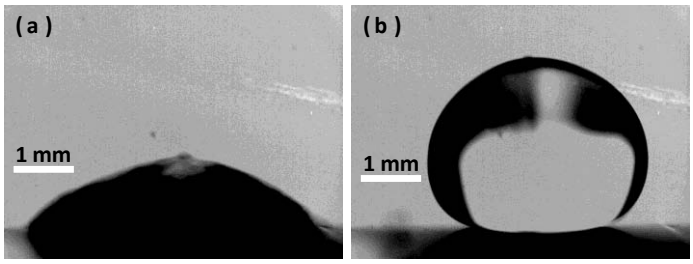

FIGURE 5: (a) Wetting (Wenzel) droplet boiling at low superheat (ΔT = 19˚C) (b) Non-wetting (Cassie) droplet (ΔT = 90˚C, $V \approx$ 24 µL droplet) suspended on top of the pillars on a heated microstructured surface.

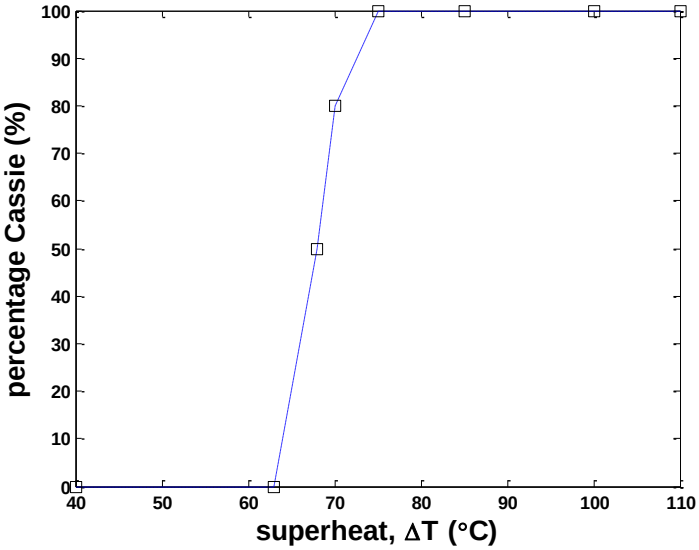

FIGURE 6: Percentage of successfully deposited Cassie droplets ($V \approx$ 15 - 25 µL) as a function of superheat on a microstructured inherently hydrophilic surface.

A sample experiment detailing the experimental methodology is shown in Fig. 7. A superheat of 94˚C was required initially to deposit a Cassie droplet. This implies that the forces involved during droplet deposition are larger than the forces involved after deposition. During deposition, as the droplet contacts the substrate, the center of gravity decelerates rapidly initiating a shock wave that generates an enormous pressure when water is compressed behind the shock wave envelope [18]. This pressure, referred to as the water hammer pressure, scales with the time derivative of the inertia term in the Navier-Stokes equation [18, 19]. The rapid deceleration of the droplet and the resulting force due to the water hammer effect along with the weight of the droplet, the surface tension force, and the force due to the dynamic pressure act downward to induce wetting. The only forces acting to prevent wetting and suspend the droplet on top of the pillar array structure is that due to the high pressure region created by the viscous resistance to the radially escaping vapor within the tiny gap between the pillar-top and pillar-base. Of the four wetting forces, water hammer and dynamic pressure act only during the initial stages and dissipate quickly after droplet deposition. The effect of dynamic pressure can be avoided to a great extent by gently depositing the droplet. However, it is very difficult to avoid the effect of water hammer in practical experiments. Moreover, water hammer ($\sim O[\rho uc]$) is usually significantly larger in magnitude than all the other forces (*e.g.* dynamic pressure ($\sim O[\rho u^2]$) involved in the process [18, 19]. We believe that it is this short-lived water hammer pressure generated during droplet deposition on the surface that required an initially higher superheat at the start of the experiment. The reduction in the downward wetting force after deposition (only surface tension and weight remain) consequently lowered the superheat requirement to maintain an already deposited Cassie droplet.

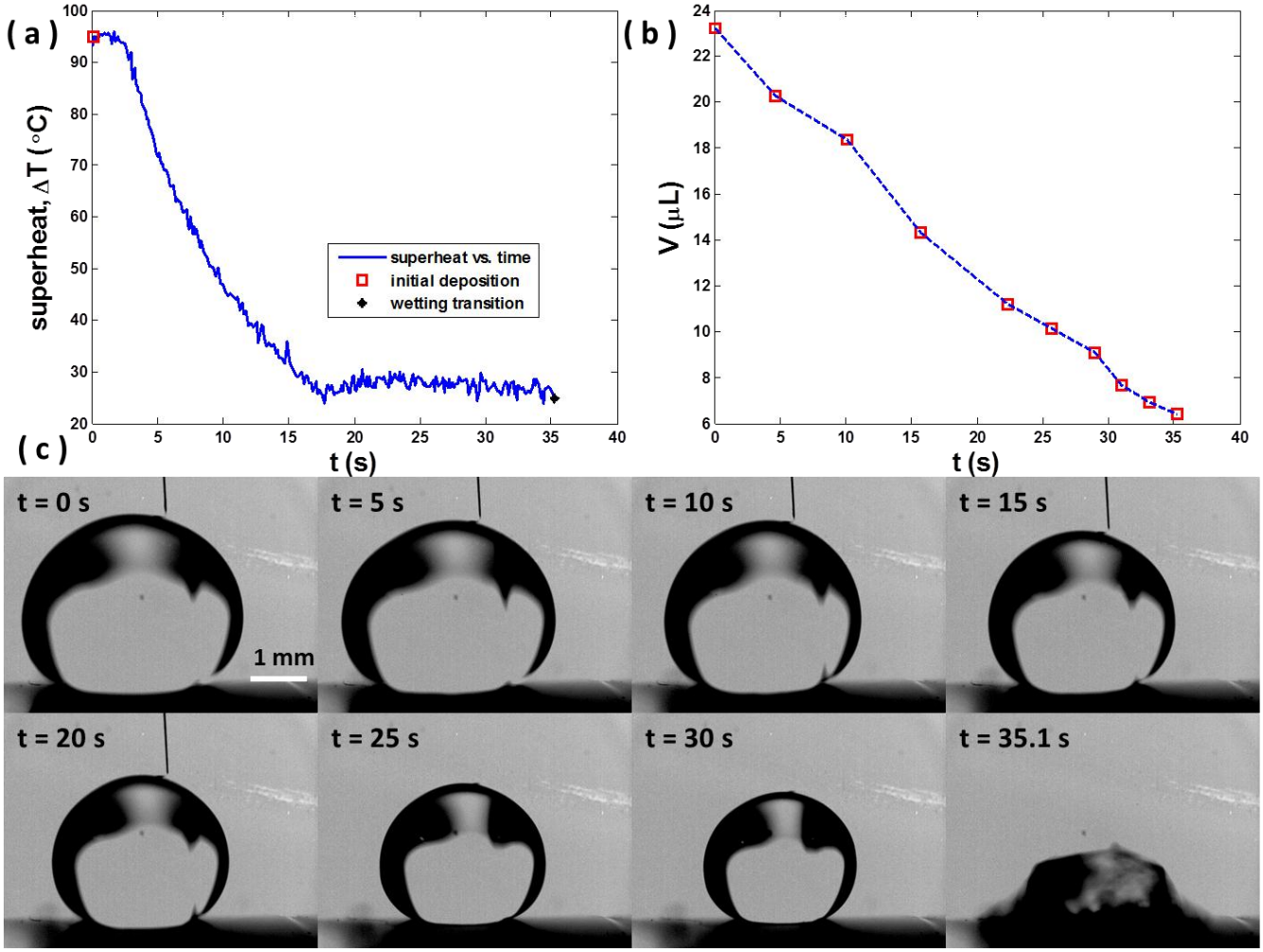

FIGURE 7: (a) Typical superheat as a function of time for a droplet deposited on a superheated microstructured surface, (b) Corresponding droplet volume as a function of time, (c) Time lapse images of an evaporating droplet at 5 s intervals (steady state temperature was reached 17 s after deposition, and the transition from the Cassie to the Wenzel state occurred at t = 35.1 s corresponded to ΔT = 26˚C, and V = 6.4 μL). The 25 μm gold wire used to keep the droplet in position during the experiment is visible in some (out of focus for the rest) of the images.

The droplets at high superheats (94˚C) were very dynamic and difficult to image. Moreover, the water hammer effect is not clearly understood and hence it was difficult to quantify the forces acting on the droplet at deposition. To counter these shortcomings, once deposited, the 3-way switch was toggled and the substrate was allowed to cool down (3-18 sec) to attain a steady state at a lower superheat of 26˚C as shown in Fig. 7a. The superheat was then maintained at this value as the droplet evaporated until transition occurred at 35.1 seconds (Fig. 7a and 7c). A plot of droplet volume measured from the acquired images (Fig. 7c) is shown in Fig. 7b. The volume of the droplet at transition to the Wenzel state was ~ 6.4 µL. This experimentally observed transition temperature is much lower than the Leidenfrost temperature reported for smooth flat surfaces [20].

MODELING

To explain the observations, we developed a simple quasi-steady 1-D lubrication model which is valid after the dynamic and water hammer pressures have dissipated and a steady state temperature was achieved (>18 s on Fig. 7a). A schematic of the evaporating Cassie droplet on top of the structured surface is shown on Fig. 8. The temperature at the droplet base (or pillar top) is assumed to be the saturation temperature of water at ambient pressure. Uniform evaporation throughout the droplet base was assumed. The apparent contact angle of the droplet was estimated using the Cassie-Baxter equation for composite surfaces [21, 22], silicon pillars and water vapor in this case.

$$\cos\,\theta_c = -1 + \phi_s\left(1 + \cos\,\theta_f\right), \tag{2}$$

Here, θ_f and θ_c are the intrinsic contact angle on a flat surface and the apparent contact angle on the composite surface, respectively. The apparent contact angle for the current geometry was calculated to be θ_c = 161^o using an intrinsic contact angle of 38^o for a smooth flat silicon surface and solid fraction of ϕ_s = 0.03. The calculated apparent contact angle from the Cassie-Baxter equation is different from the experimentally measured apparent contact angle θ_{app} of 149˚ (Fig. 4). The difference between the experimental and the predicted values of the apparent contact angle can be attributed to measurement uncertainties and the fact that Eq. 2 is valid for a sessile droplet in equilibrium while the droplets in the current study are evaporating and hence a receding contact angle. Based on the apparent contact angle defined by Eq. 2, a relation between the base radius R and droplet major radius R_o can be established from geometry as,

$$R = R_0 \sin\theta_c. \tag{3}$$

The effect of gravity on the shape of the droplet can be ignored since the Bond number is less than unity at transition ($Bo \approx 0.2$, for the particular case shown on Fig. 7 where the droplet transitioned at 6.4 µL, which corresponds to a droplet radius of 1.2 mm).

We further assume that the conducted heat is completely utilized to induce uniform evaporation at the liquid/vapor interface of the droplet basal area. The vapor escapes from the droplet base with velocity v in the z-direction and could be related to the heat conduction through the composite media as

$$v = -\frac{k_{eff}\Delta T_p}{\rho_{vap} h_{fg} h}, \tag{4}$$

where ρ_{vap} and h_{fg} are the density of vapor and the latent heat of vaporization respectively, ΔT_p is the temperature difference between the pillar top and the pillar base, and k_{eff} is the effective thermal conductivity of the porous media composed of the silicon pillars and the water vapor and is estimated by Eq. 5 from [23]

$$k_{eff} = (1 - \phi_s)k_{vap} + \phi_s k_{si}, \tag{5}$$

where k_{vap} and k_{Si} are the thermal conductivities of water vapor and Silicon at saturation conditions (k_{si} at 100˚C is ~ 105 W/m-k) [24].

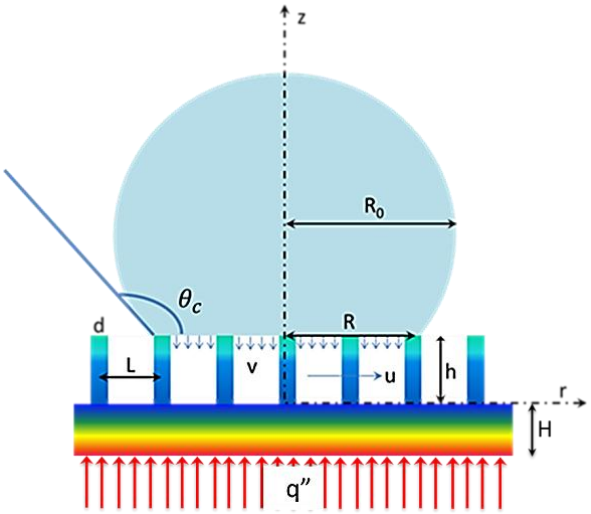

FIGURE 8: Schematic of a non-wetting Cassie droplet on a superheated microstructured surface. The apparent contact angle is θ_c, droplet major radius is R_0, and the base radius is R. Heat is conducted through the substrate and the porous pillar-vapor medium to induce evaporation at the three-phase contact line. As the vapor escapes out radially (r = 0 to r = R) through the porous medium, a pressure gradient is created that supplies the anti-wetting force required to suspend the droplet on the pillar top. The force due to the pressure gradient balances the surface tension force and the weight of the droplet that act to induce wetting.

Considering that h / R << 1, it is assumed that the vapor velocity v in the z-direction is small compared to the radial vapor velocity u (*i.e.*, v/ u << 1, here v is constant because of

the previous assumption of uniform evaporation). The continuity equation at any radial position r under the droplet base can then be written as

$$\int_0^h u\,(2\pi r)dz = \pi r^2 v. \tag{6}$$

Combining Eqs. 4 and 6, we obtain a relation between the velocity and temperature difference between the pillar base and pillar top as

$$\int_0^h u\,dz = -\frac{k_{eff}\Delta T_p}{2\rho_{vap}h_{fg}}\frac{r}{h}. \tag{7}$$

Since $h / R << 1$, further assumptions can be made that simplify the analysis as follows: (1) the viscous loss is dominated by velocity gradients in the z-direction *i.e.*, the radial velocity is a function of z-direction only, u (z), (2) momentum changes in the axial direction can be neglected, and (3) the pressure depends only in the radial direction, $\partial p/\partial z = 0$. Using these assumptions, the classical momentum equation for porous media can be simplified to Brinkman equation [25],

$$\frac{\partial^2 u}{\partial z^2} = \frac{\varepsilon}{\mu}\frac{dP}{dr} + \frac{\varepsilon u}{K}, \tag{8}$$

where ε is the porosity and K is the permeability of the porous media. The permeability was calculated using an asymptotic expression valid for flow through dilute pillar arrays, $\phi_s \leq 0.25$ [26]. Equation 8 is then solved by applying the no-slip boundary conditions ($u = 0$) at the pillar base ($z = 0$) and pillar top ($z = h$). An average radial velocity, which depends only on r, can then be found by integrating the velocity profile u (r, z), obtained from Eq. 8 in the z-direction from the base ($z = 0$) to the tip ($z = h$) of the pillar. This average radial velocity is then equated with the average velocity obtained previously from Eq. 7 using energy balance to find the pressure profile along the radial direction,

$$P(r) - P_{amb} = \frac{\mu_{vap}k_{eff}\Delta T_p(R^2 - r^2)}{4\varepsilon h\rho_{vap}h_{fg}\left(\dfrac{2\tanh\left(\dfrac{h}{2}\sqrt{\dfrac{\varepsilon}{K}}\right)}{\left(\dfrac{\varepsilon}{K}\right)^{3/2}} - \dfrac{hK}{\varepsilon}\right)} \tag{9}$$

where P_{amb} is the ambient pressure and P (r) is the pressure at a radial distance r from the center of the droplet base ($r = 0$). The upward anti-wetting force on the droplet F_{up} was calculated by integrating the pressure profile from Eq. 9 over the droplet base area from $r = 0$ to $r = R$,

$$F_{up} = \frac{\pi\varepsilon\mu_{vap}k_{eff}\Delta T_p}{8\rho_{vap}h_{fg}}\left(\frac{2\tanh\left(\dfrac{h}{2}\sqrt{\dfrac{\varepsilon}{K}}\right)}{\left(\dfrac{\varepsilon}{K}\right)^{3/2}} - \frac{hK}{\varepsilon}\right)^{-1}\frac{R^4}{h}. \tag{10}$$

As can be seen from Eq. 10, the upward force which resists the droplet from wetting the substrate is dependent on fluid properties (which in turn depend on the temperature and pressure of the droplet), the geometry of the microstructured surface including the porosity and permeability, the effective thermal conductivity of the composite porous media, and the droplet base radius. This strong dependence on droplet base radius ($F_{up} \propto R^4$) is important in explaining the experimental results. After dynamic and water hammer pressures have dissipated, the downward wetting force on the droplet F_{down} due to the weight of the droplet and the surface tension force is given by

$$F_{down} = \rho_{liq}Vg + N\pi d\sigma\cos\theta_f, \tag{11}$$

where V is the droplet volume, ρ_{liq} is the density of liquid water at saturation temperature, d is the pillar diameter, and $N = \pi R^2/l^2$ is the number of pillars in contact with the droplet base.

The downward wetting force due to the surface tension is usually more than one order of magnitude higher than that due the weight. As a result, the downward force can be roughly approximated to depend on the square of droplet base radius ($F_{down} \propto R^2$). Therefore, as the droplet shrinks in size, the anti-wetting force due to pressure decreases at a faster rate ($F_{up} \propto R^4$) than the opposing wetting forces ($F_{down} \propto R^2$) as shown in Eqs. 10 and 11. Comparing the two forces together, it is clearly evident that the anti-wetting (upward) force dominates at larger volumes requiring lower superheat. The temperature difference required to sustain a droplet in the Cassie state is obtained by equating the wetting and anti-wetting forces,

$$\Delta T_p = \frac{\rho_{liq}Vg + \sigma\pi Nd\cos\theta_f}{\dfrac{\pi\varepsilon\mu_{vap}k_{eff}}{8\rho_{vap}h_{fg}}\left(\dfrac{2\tanh\left(\dfrac{h}{2}\sqrt{\dfrac{\varepsilon}{K}}\right)}{\left(\dfrac{\varepsilon}{K}\right)^{3/2}} - \dfrac{hK}{\varepsilon}\right)^{-1}\dfrac{R^4}{h}} \tag{12}$$

Equation 12 estimates the temperature difference between the pillar base and pillar top that is required to maintain a Cassie droplet. An additional temperature drop between the pillar base and the backside of the substrate is required to match the experimentally measured wall temperature with the model prediction. Incorporating this additional temperature drop across the sample thickness (~ 620 μm thick silicon), the overall temperature drop from the backside of the sample to the pillar top is

$$\Delta T = \Delta T_p \left(1 + \frac{Hk_{eff}}{hk_{Si}}\right). \quad (13)$$

Equation 13 provides an estimate for the overall superheat ΔT required for suspending a Cassie droplet. The superheat increases as the droplet gets smaller in size ($\Delta T \propto R^{-2}$), consistent with experimental observations. The experimentally measured superheats and the model prediction are shown in Fig. 9. The solid black line is the model prediction based on the apparent contact angle as obtained from the Cassie-Baxter equation (161˚) while the dotted blue line is the model prediction based on the experimentally measured contact angle (149˚, Fig. 4). As can be seen, estimating the apparent contact angle correctly is key in predicting the correct superheat required for the Cassie-to-Wenzel transition. Nonetheless, the simple 1-D lubrication model qualitatively captures the transition mechanism, showing good agreement with the trend in the experimental data.

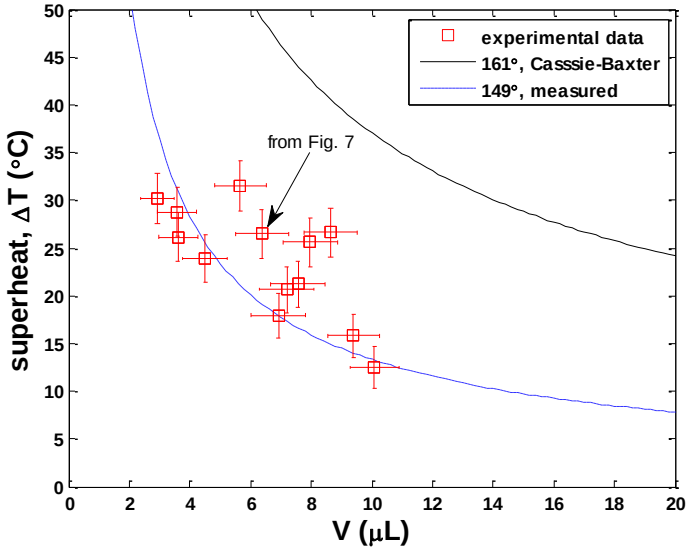

FIGURE 9: Relationship between superheat and transition volume of a droplet deposited on the superheated microstructured surface shown in Fig. 2a.

CONCLUSIONS

Evaporation-induced Cassie-to-Wenzel transition of water droplets on super-heated superhydrophilic microstructured surfaces have been investigated. We demonstrated that a superhydrophilic surface at room temperature can take on the characteristics of a superhydrophobic surface if the substrate is superheated. Experiments performed at steady state temperatures have shown that a relatively smaller superheat is required to sustain an already suspended droplet in the Cassie state on a superhydrophilic surface than that required when initially depositing the droplet. The relatively higher superheat required for the initial deposition of a Cassie droplet is hypothesized to be the result of a transient water hammer pressure that develops during the droplet deposition process. We have shown that a single surface can exhibits both extremes of wettability (superhydrophilicity and superhydrophobicity) and that an increasing superheat is required to maintain a Cassie droplet as the droplet radius decreases. A model was developed to understand this steady-state behavior at capillary length scales and shows good agreement with the experiments. This work offers new insights into the design of structured surfaces for phase-change heat transfer applications.

ACKNOWLEDGMENTS

The authors gratefully acknowledge funding support from ONR with Mark Spector as program manager. The authors would like to acknowledge the MIT Microsystems Technology Lab for fabrication staff support, help and use of equipment. R.R. acknowledges support from Battelle's National Security Global Business, and R.E. acknowledges support from the Irish Research Council for Science, Engineering, and Technology, cofunded by Marie Curie Actions under FP7.

REFERENCES

[1] Quéré, D., 2008, "Wetting and Roughness," Annu. Rev. Mater. Res., **38**, pp. 71-99.

[2] Bico, J., Thiele, U., and Quéré, D., 2002, "Wetting of Textured Surfaces," Colloids and Surfaces A: Physicochemical and Engineering Aspects, **206**(1-3), pp. 41-46.

[3] Zheng, L., Wu, X., Lou, Z., and Wu, D., 2004, "Superhydrophobicity from Microstructured Surface," Chinese Science Bulletin, **49**(17), pp. 1779-1787.

[4] Norton FJ. 1945. U.S. Patent No. 2,386,259.

[5] Gao, L., and McCarthy, T. J., 2007, "A Commercially Available Perfectly Hydrophobic Material (θA/θR= 180°/180°)," Langmuir, **23**(18), pp. 9125-9127.

[6] Herminghaus, S., 2000, "Roughness-Induced Non-wetting," EPL (Europhysics Letters), 52, p. 165.

[7] Patankar, N. A., 2004, "Transition Between Superhydrophobic States on Rough Surfaces," Langmuir, **20**(17), pp. 7097-7102.

[8] Callies, M., and Quéré, D., 2005, "On Water Repellency," Soft matter, **1**(1), pp. 55-61.

[9] Reyssat, M., Yeomans, J., and Quéré, D., 2008, "Impalement of Fakir Drops," EPL (Europhysics Letters), **81**, p. 26006.

[10] Quéré, D., Lafuma, A., and Bico, J., 2003, "Slippy and Sticky Microtextured Solids," Nanotechnology, **14**, p. 1109.

[11] Bormashenko, E., Pogreb, R., Whyman, G., and Erlich, M., 2007, "Cassie-Wenzel Wetting Transition in Vibrating Drops Deposited on Rough Surfaces: Is the Dynamic Cassie-Wenzel Wetting Transition a 2D or 1D Affair?," Langmuir, **23**(12), pp. 6501-6503.

[12] Bormashenko, E., Pogreb, R., Whyman, G., and Erlich, M., 2007, "Resonance Cassie-Wenzel Wetting Transition for Horizontally Vibrated Drops Deposited on a Rough Surface," Langmuir, **23**(24), pp. 12217-12221.

[13] Han, Z., Tay, B., Tan, C., Shakerzadeh, M., and Ostrikov, K., 2009, "Electrowetting Control of Cassie-to-Wenzel Transitions in Superhydrophobic Carbon Nanotube-based Nanocomposites," ACS nano, **3**(10), pp. 3031-3036.
[14] Krupenkin, T. N., Taylor, J. A., Wang, E. N., Kolodner, P., Hodes, M., and Salamon, T. R., 2007, "Reversible Wetting-dewetting Transitions on Electrically Tunable Superhydrophobic Nanostructured Surfaces," Langmuir, **23**(18), pp. 9128-9133.
[15] Liu, G., Fu, L., Rode, A. V., and Craig, V. S. J., 2011, "Water Droplet Motion Control on Superhydrophobic Surfaces: Exploiting the Wenzel-to-Cassie Transition," Langmuir, **27**, pp. 2595-2600.
[16] Tsai, P., Lammertink, R. G. H., Wessling, M., and Lohse, D., 2010, "Evaporation-triggered Wetting Transition for Water Droplets upon Hydrophobic Microstructures," Physical review letters, **104**(11), p. 116102.
[17] Zhang, T., Wang, J., Chen, L., Zhai, J., Song, Y., and Jiang, L., 2011, "High-Temperature Wetting Transition on Micro- and Nanostructured Surfaces," Angewandte Chemie International Edition, **50**(23), pp. 5311-5314.
[18] Deng, T., Varanasi, K. K., Hsu, M., Bhate, N., Keimel, C., Stein, J., and Blohm, M., 2009, "Nonwetting of Impinging Droplets on Textured Surfaces," Applied Physics Letters, **94**(13), p. 133109.
[19] Kwon, H.-M., Paxson, A. T., Varanasi, K. K., and Patankar, N. A., 2011, "Rapid Deceleration-Driven Wetting Transition during Pendant Drop Deposition on Superhydrophobic Surfaces," Physical review letters, **106**(3), p. 036102.
[20] Gottfried, B., Lee, C., and Bell, K., 1966, "The Leidenfrost Phenomenon: Film Boiling of Liquid Droplets on a Flat Plate," International Journal of heat and mass transfer, **9**(11), pp. 1167-1188.
[21] Bico, J., Marzolin, C., and Quéré, D., 1999, "Pearl Drops," EPL (Europhysics Letters), 47, p. 220.
[22] Cassie, A., and Baxter, S., 1944, "Wettability of Porous Surfaces," Trans. Faraday Soc., **40**(0), pp. 546-551.
[23] Peterson, G., 1994 "*An Introduction to Heat Pipes: Modeling, Testing and Applications*," Wiley, New York, pp.99.
[24] Shanks, H., Maycock, P., Sidles, P., and Danielson, G., 1963, "Thermal Conductivity of Silicon from 300 to 1400 K," Physical Review, **130**(5), p. 1743.
[25] Brinkman, H., 1947, "Applied Sci. Research A 1, 27 (1947)," Proc. Netherl. Acad. Sci. Amsterdam, 50, p. 618.
[26] Sangani, A., and Acrivos, A., 1982, "Slow Flow Past Periodic Arrays of Cylinders with Application to Heat Transfer," International journal of Multiphase flow, **8**(3), pp. 193-206.